15th AIAA Computational Fluid Dynamics Conference
11-14 June 2001 Anaheim, CA

A01-31087

AIAA-2001-2602

Reduced Order Modeling for a One-Dimensional Nozzle Flow with Moving Shocks

David J. Lucia*
Air Force Institute of Technology, WPAFB, OH 45433

Paul I. King†
Air Force Institute of Technology, WPAFB, OH 45433

Philip S. Beran‡
Air Force Research Laboratory, WPAFB, OH 45324

Mark E. Oxley§
Air Force Institute of Technology, WPAFB, OH 45433

Proper Orthogonal Decomposition (POD) has been used with great success to produce accurate Reduced Order Models (ROMs) for low-speed flow fields. The application of POD/ROM to low-speed flow control, aeroelastic analysis, and iterative design is currently an active field of research. The goal of this paper is to analyze the utility of POD/ROM for accurate modeling of high-speed flows with moving shock waves. The potential for the use of POD in high-speed design analysis and control applications warrants this inquiry. The challenge to using POD for high-speed flows is presented by the presence of discontinuities in the flow field. The ability of POD/ROM to model a high-speed quasi 1-D nozzle flow is analyzed. The quasi 1-D nozzle contains a standing shock which can be moved by varying boundary parameters or the ratio of specific heats (γ) in the flow field. The accuracy of POD/ROM in modeling this flow field is quantified. The robustness of the POD/ROM to varying flow parameters is explored. Finally, a domain decomposition approach for reduced order modeling of shocked flows with POD is developed, and its performance is quantified.¶

Nomenclature

$A(x)$	Nozzle cross sectional area
E	Vector of x-axis fluxes
E_t	Total energy
G	Vector valued function for overlapping domains
I	Identity matrix
M	Number of DOFs for reduced order model
Q	Number of snapshots used in POD/ROM
P, ρ	Pressure, density
$R()$	Right-Hand-Side or nonlinear portion of Euler equations
t	Time
S	Matrix of flow field data, or snapshots
T	Vector mapping overlapping variables
u	Fluid velocity
V	Matrix of eigenvectors of S^TS
$\underline{w}, \underline{\widehat{w}}$	Full or reduced order vector for a single fluid variable
x	Spatial coordinate along axis of nozzle
$\underline{x}, \underline{\widehat{x}}$	Full and reduced order vector of flow variables
$\underline{y}, \underline{\widehat{y}}$	Flow variables augmented with LaGrange multiplier
$\underline{Z}$	Vector of forcing terms
γ	Ratio of Specific Heats
Λ	Matrix of singular values of S^TS
λ	LaGrange multiplier
Ψ	Reduced order mapping matrix

Subscripts

DD	Domain decomposition
$S\sharp$	Section number "$\sharp$" within domain
λ	Overlapping domains

Superscripts

n	Index to increment discrete time steps
ν	Index to increment Newton iterations

*Major, USAF, Doctoral Candidate, AIAA Member.
†Associate Professor, Member AIAA
‡Senior Research Engineer, Senior Member AIAA
§Associate Professor
¶The views expressed in this article are those of the authors and do not reflect the official policy or position of the United States Air Force, the Department of Defense, or the U.S. Government.

Introduction

The desire to use Computational Fluid Dynamics (CFD) in design analysis has motivated a search for faster CFD codes. The primary cause of long run times for CFD codes is the large number of degrees of freedom (DOFs) from the discretized computational mesh. Proper Orthogonal Decomposition (POD) of CFD flow simulations was introduced in the mid 1990s to reduce the number of DOFs of CFD solvers. The literature refers to such POD based fluid models as POD Reduced Order Models (ROMs), where the term "order" is used to imply the number of degrees of freedom.

Currently, POD/ROMs are being used for design analysis and nonlinear control of low-speed flows. POD has been successfully applied to low-speed nonlinear aeroelastic problems.[1] POD has also been used for low-speed airfoil design.[2] Computers using the POD reduced order models can produce data fast enough to enable some types of flow control for general flow fields.[3]

The goal of this research is to explore the use of POD/ROM on a 1-D high-speed flow field with a strong, moving shock. The challenge in using POD for high-speed flow fields is presented by the presence of moving shock waves in such flows. It will be shown that current techniques for generating POD/ROMs, as used for low speed analysis, will not generate useful ROMs for the high-speed case with moving shocks. POD/ROMs generated in this manner will require too much data to be useful, and they cannot be relied upon to track changes in shock location as the boundary conditions or flow parameters are changed. Instead, a shock capturing technique will be developed that exploits POD and also accurately treats moving shock waves. This technique will decompose the solution domain to isolate regions that contain shocks. A reduced order model for each region will be developed independently, and the solution for the entire domain will be formed by linking the boundaries of each region to systematically solve for the flow field.

Quasi 1-D Nozzle

An analysis of POD/ROM for high-speed flows with moving shocks was conducted on an inviscid 1-D flow field. Specifically, a quasi 1-D divergent nozzle was used as the model problem as shown in Figure 1. A quasi 1-D nozzle accounts for the area change of the nozzle by inserting a forcing function into the 1-D Euler equations. The resulting solution is interpreted as the flow field at the centerline of the nozzle. A numerical solver based on Roe's scheme for this simplified flow field was used as the "full order solution" from which various POD/ROMs were generated and compared.

For unsteady one-dimensional flow in a duct of variable (but known) cross-sectional area, the Euler equations (in conservation form) reduce to the equation set given below.[4]

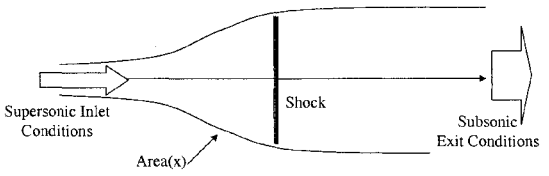

Fig. 1 Quasi 1-D Nozzle

$$U_t + E_x = Z$$

$$U = \begin{bmatrix} \rho A \\ \rho u A \\ \rho E_t A \end{bmatrix} \quad (1)$$

$$E = \begin{bmatrix} \rho u A \\ (\rho u^2 + P)A \\ (\rho E_t + P)uA \end{bmatrix} \quad (2)$$

$$Z = \begin{bmatrix} 0 \\ -P\frac{dA}{dx} \\ 0 \end{bmatrix} \quad (3)$$

Here ρ is density, ρu is x-direction momentum, P is pressure, and E_t is total energy per unit mass. These three fluid variables are functions of both space and time. The following profile was used for nozzle area.

$$A(x) = 1.398 + 0.347\tanh(0.8x - 4)$$

Roe's scheme[5] was used to explicitly solve the entire flow field by discretizing the spatial domain into a fine grid, and time marching from a known initial condition via small time steps. The inlet was at $x = 0$, and the inlet boundary conditions (non-dimensional) were $\rho_{in} = 0.5020$, $u_{in} = 1.299 \Rightarrow (\rho u)_{in} = 0.6521$, and $Et_{in} = 1.3758$. The nozzle exit was at $x = 10$, and the exit boundary condition was $\rho_{out} = 0.776$. The fluid modeled was air with $\gamma = 1.4$. For these conditions, a shock forms in the nozzle at $x = 4.816$.[4]

Proper Orthogonal Decomposition

POD is a technique to identify a small number of DOFs that adequately reproduce the behavior of a large DOF CFD flow field representation. The greater the reduction in DOFs, the faster the computer produces a solution. A summary of POD is as follows.

Let $\underline{w}$ be a time varying vector representing one of the three fluid variables in U from equation (1). Each vector location holds the fluid variable value at a single grid point. For this fluid variable, consider the portion of the Roe's scheme flow solver that models the flux term E_x and the forcing function Z. Denote this as a nonlinear operator R acting on $\underline{w}$. $R(\underline{w})$ is the outcome of a function call to the Roe's scheme solver in the

computer code for the full order solution. Using this notation, the numerical Roe's scheme solver for this fluid variable behaves as depicted in equation (4).

$$\frac{d\underline{w}}{dt} = R(\underline{w}) \tag{4}$$

POD produces a linear transformation Ψ between the full order solution $\underline{w}$, and the reduced order solution for this fluid variable $\underline{\widehat{w}}$ as follows. Note that Ψ is not time varying, where $\underline{w}$ and $\underline{\widehat{w}}$ are functions of time t.

$$\underline{w}(t) = \Psi\underline{\widehat{w}}(t)$$

Ψ is constructed by collecting observations of the full order solution $\underline{w}$ at different time intervals throughout the explicit time integration of the Roe solver. These observations are called snapshots and are generally collected prior to reaching steady state to minimize linear dependence. This time integration and snapshot generation procedure is sometimes referred to as the POD training period.

A total of Q snapshots (usually about 20 or 30) are collected of the full order solution vector length N. These snapshots are compiled into a $N \times Q$ matrix S, known as the snapshot matrix. The reduced order solution $\underline{\widehat{w}}$ will be an optimally convergent representation of the full order variable if the mapping function Ψ is developed as follows.[6]

$$\begin{aligned} S^T S V &= V\Lambda \\ \Psi &= SV \end{aligned}$$

Here V is the matrix of eigenvectors of $S^T S$, and Λ is the corresponding diagonal matrix of eigenvalues (also called singular the values of S). To eliminate redundancy in the snapshots, the columns of V corresponding to very small eigenvalues in Λ are truncated. The matrix of eigenvalues Λ is also resized to eliminate the rows and columns corresponding to the zero eigenvalues. If $Q-M$ columns of V are truncated, the resulting reduced order mapping Ψ will be an $N \times M$ matrix. This reduced order mapping is a modal representation of the flow field. The modes are the columns of Ψ which are discretized spatial functions fixed for all time. The vector $\underline{\widehat{w}}$ is a time dependent set of unknown coefficients that represent the contribution of each mode to the solution at the given time.

The final step is to recast the governing equations to solve for the coefficients. Galerkin projection is commonly used in the literature,[6] but a non-Galerkin approach is used in this analysis for simplicity. The non-Galerkin approach uses the original dynamics equation and a forward difference approximation to yield the following reduced order flow solver.[7] Here n represents discretized time steps, and the pseudo inverse is used assuming modal truncation is employed making V a non-square matrix.

$$\frac{d\underline{w}}{dt} = R(\underline{w}) \Rightarrow \underline{w}^{n+1} = \underline{w}^n + \Delta t R(\underline{w})$$

$$\underline{\widehat{w}}^{n+1} = \underline{\widehat{w}}^n + \Delta t \Lambda^{-1}(V^T V)^{-1} V^T S^T R(\underline{w}^n) \tag{5}$$

The POD/ROM reduces each flow variable from N to M, where M is the number of POD modes. This method of order reduction in equation (5) relied on the full order function evaluation at each flow field integration step. As such, the order of each integration step was not actually reduced. However, this reduction technique can greatly increase the time step size allowed for stability. Therefore, the total number of time steps required for the explicit time accurate solver to reach steady state is significantly reduced.

The solution to the Euler equations in 1-D requires simultaneous solution for three fluid variable vectors $\underline{w}(t)$. The corresponding vector for each flow variable was stacked into a single vector denoted $\underline{x}(t)$ representing the flow field as a function of time. The portion of the Roe's scheme flow solver that models the flux term E_x and the forcing function Z for all three fluid variables was stacked in the same manner and denoted $F(\underline{x}(t))$. Finally, the reduced order mappings for each fluid variable (S and V) were collocated as blocks into a larger reduced order mapping. This produced the following variant of equation (5) which applies to all three fluid variables simultaneously.

$$\underline{\widehat{x}}^{n+1} = \underline{\widehat{x}}^n + \Delta t \Lambda^{-1}(V^T V)^{-1} V^T S^T F(\underline{x}^n) \tag{6}$$

Shocks with POD

This section presents results for POD/ROMs generated from snapshots of the quasi 1-D nozzle flow field. No special treatment of the shock was provided. Rather, POD was applied much like it has been applied to low-speed flow fields.

A POD/ROM was constructed using 100 snapshots taken from time integration of the Roe solver for the quasi 1-D nozzle problem at $1s$ intervals. For the chosen initial conditions, the solver very closely reached steady state by $100s$. For this experiment, an evenly spaced 63 grid point mesh was used. Since the number of snapshots outnumbered the DOFs in this case, there were many zero eigenvalues for $S^T S$ which had to be truncated to create the POD/ROM.

The chosen initial condition $(\rho(x,0),\ (\rho u)(x,0),\ E_t(x,0))$ was simply a linear function of x connecting the inlet and exit boundary conditions with reasonably close estimates for the final values of the unspecified inlet and exit flow variables. For example, ρ was specified only at the nozzle exit. The initial condition for density was a line connecting this specified exit value

with an approximation of the steady state value of ρ at the inlet. As repeated integrations were applied to this initial condition, the inlet values $\rho(0,t)$ were unconstrained, but the exit value $\rho(x_f,t)$ stayed fixed. The resulting flow field took a wide range of functional forms; from smooth linear functions to discontinuous ones.

The flow field dynamics during the $100s$ time integration are summarized as follows. For brevity, density is the lone fluid variable that will be discussed. The first $7s$ of this trajectory are shown in Figure 2. Each line is a snapshot of the full order density solution at $1s$ intervals in time. Notice that the shock wave formed in the first $7s$, and it formed about 1 distance unit down stream ($x \approx 5.8$) of the steady state shock location ($x = 4.816$).

The next $23s$ of the trajectory are shown in Figure 3. In this portion of the trajectory the shock wave moved up stream to $x \approx 4.3$, which was well up stream of the final steady state shock location.

The final portion of the trajectory is depicted in Figure 4. The shock locations underwent smaller oscillations and finally settled at the steady state value of $x = 4.816$.

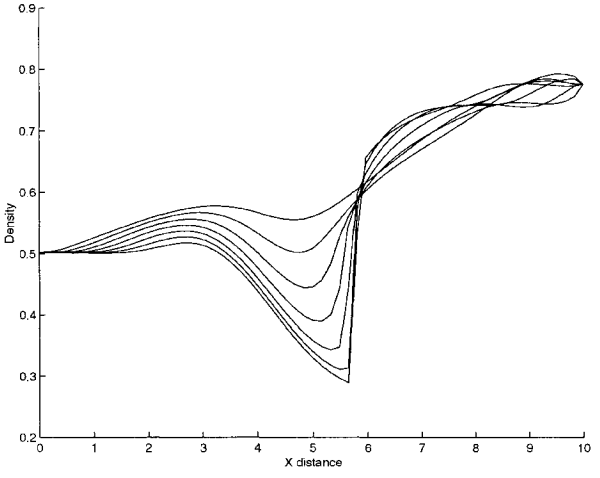

Fig. 2 Density Function $t = 0 \rightarrow 7s$

The resulting POD/ROM was able to reproduce the flow solution from which it was generated, including the shock motion. An exceptionally good representation was obtained using 58 total modes generated from the set of 100 snapshots (20 modes for ρ, 19 modes for ρu, and 19 modes for E_t). Every metric considered indicated a close adherence to the true spatial solution for each fluid variable at each point in time. The largest L_{max} for any fluid variable was only 1.15%. This indicates that there is no place or time that the reduced order model does not closely match the true solution. The largest L^2_{err} for any fluid variable at any time was only 0.404%, indicating that spatial features of the solution were also closely tracked for all

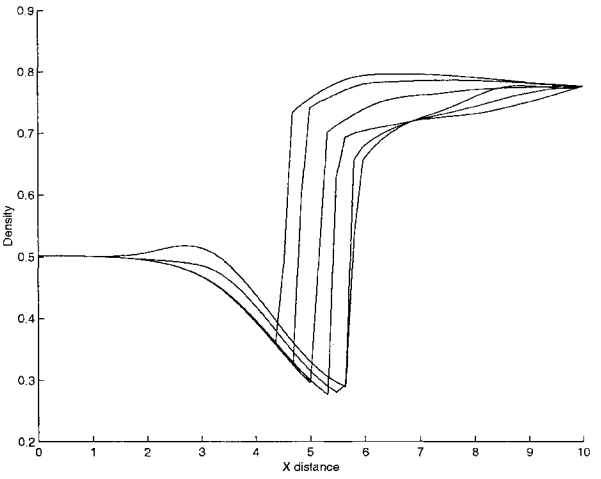

Fig. 3 Density Function $t = 7 \rightarrow 30s$

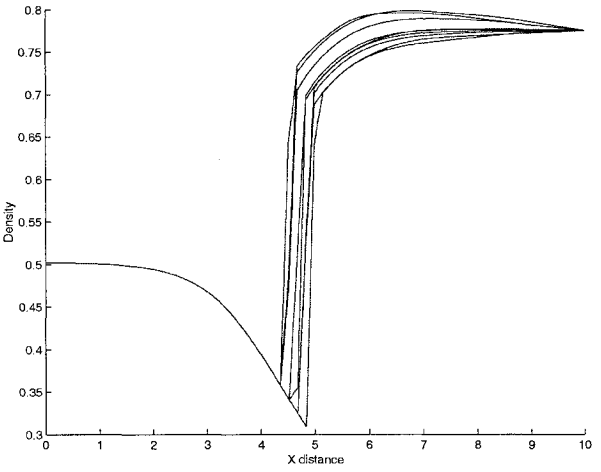

Fig. 4 Density Function $t = 30 \rightarrow 100s$

time. POD/ROM provided exceptional solution accuracy while reducing the order from 189 degrees of freedom to 58.

Depending on the application, errors of 5% on the average might be acceptable. This was achieved with about 45 modes (15 modes for ρ, 15 modes for ρu, and 15 modes for E_t). From 36 to 28 modes, the reduced order model generated a reasonable approximation of the full order solution for most of the trajectory. Reduced order models below 25 modes were of questionable use.

Also, the POD/ROM got worse when too many modes were included. The modes corresponding to very low eigenvalues captured dynamics due to machine numerics, not flow structures. Instabilities arose that prevented the reduced order model from reaching steady state when too many modes were included.

The columns of Ψ represents the basis functions(or modes) that the reduced order model uses to linearly reconstruct the time sequence of functions. These

modes are ordered by the size of their eigenvalues, with the modes contributing the most geometrically to the snapshot data occupying the earliest columns of Ψ. The initial function $\rho(x,0)$, a linear initial density function, is subtracted from each snapshot in this implementation. Thus, the modes represent the residual spatial dynamics of the time evolution. Time integration of the reduced order model sequentially updates the solution with a POD based residual. The largest 10 modes are shown below in Figure 5.

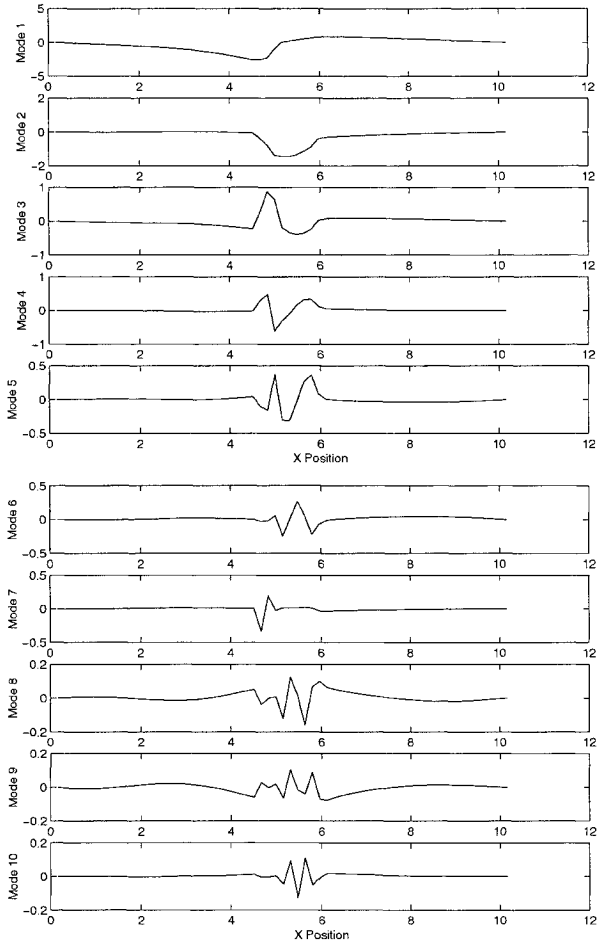

Fig. 5 Density Modes $100s$ Case $1 \rightarrow 10$

Notice that there are two distinct regions in the spatial modes for density. Between $x \approx 4.5$ and $x \approx 6$ sharp gradients and jagged transitions are prominent. Observing the y- axis scaling, the magnitude of these dynamics decreases slowly from modes 1 to 10. In contrast, outside this region a great majority of the non-zero modal contribution is contained in the first mode. Modes 8 and 9 also have a noticeable contribution to make. The major contribution to the need for a large number of modes in the POD/ROM was the region of the flow field containing the shock. Outside this range a 4 or 5 mode solution would probably have sufficed.

Initially it was unclear whether the existence of a shock in the flow field intrinsically required more modes, much like the need for a large number of Fourier sine modes to recreate a step function. As is evident in Figure 5, POD identifies discontinuous modes to track discontinuous functional behavior. Many modes were required in the region between $x \approx 4.5$ and $x \approx 6$ because of the motion of the shock wave. Few modes were required outside this region because there was not a great disparity between the initial and final states. It was the dynamics of the spatial solution in time that mattered to the POD/ROM, not the presence of spatial discontinuities in the solution.

To illustrate that relatively stationary shocks do not require a large number of modes, a POD/ROM was developed to replicate the last $30s$ of the $100s$ time integration. This comprised a sequence of functions that is nearly converged to the steady state value. For this case there was no formation of a shock from a smooth initial condition. Also, the movement of the shock was limited to two grid points. Even though the flow field contained a spatial discontinuity, it should be possible to generate an accurate POD/ROM with much fewer modes than necessary for the $100s$ case. A POD/ROM was generated from a set of 30 evenly spaced snapshots.

An exceptionally good representation of the full order trajectory was obtained using only 9 total modes (3 modes for ρ, 3 modes for ρu, and 3 modes for E_t). The largest L_{max} for any fluid variable was only 1.4% indicating that there was no place or time that the reduced order model did not closely match the true solution. The largest L^2_{err} was only 0.707%, indicating that spatial features of the solution were also closely tracked for all time. Also, a very useful reduced order model (average errors $< 5\%$) was generated from even fewer modes (2 modes for ρ, 3 modes for ρu, and 2 modes for E_t for a total of 7 degrees of freedom). This is in stark contrast to the 58 modes required for exceptionally accurate reproduction of the $100s$ case. The fact that both cases involved flow fields with discontinuities shows that the number of required modes is not intrinsically increased for shocked flows.

Consider the density modes generated for the $30s$ case shown in Figure 6. Unlike the modes for the $100s$ case, the region of sharp gradients and jagged edges is very small ($x \approx 4.75 \rightarrow 5.1$) and the amplitude diminishes quickly for increasing mode numbers. By the fourth mode, the spatial contribution of the modes are greater in the smooth regions of the flow field than for the location of the shock. Clearly the presence of the discontinuity was readily recreated with only the first three modes. This was also the case for the smooth portions of the flow field, which was recreated with three modes as well. Since the POD/ROM created discontinuous modes to represent discontinuous

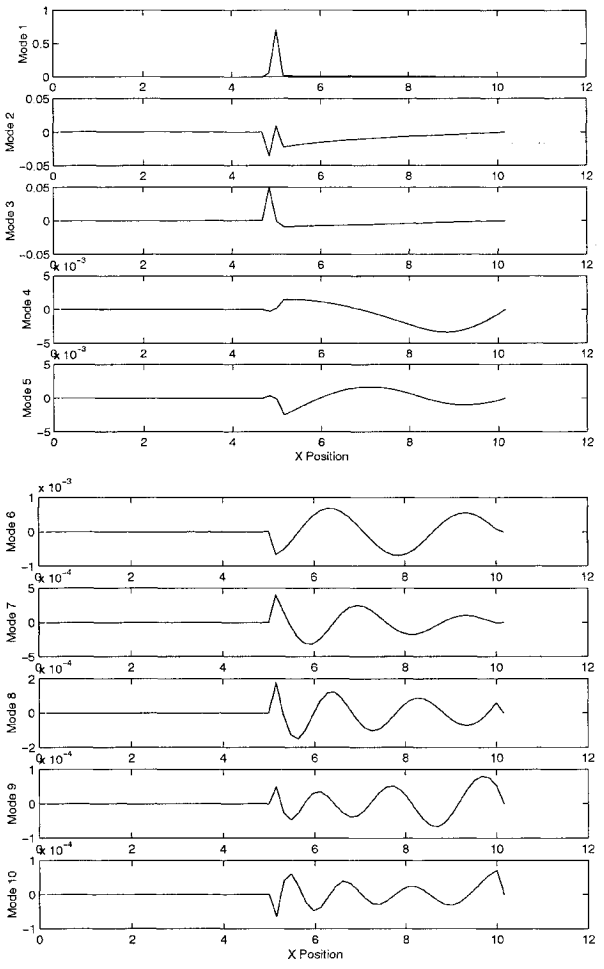

Fig. 6 Density Modes $30s$ Case $1 \rightarrow 10$

flow fields, a very few of these modes were adequate in representing the relatively stationary shock. Traditional spectral methods attempt to recreate discontinuous flow fields with smooth basis functions (complex exponentials, Chebyshev polynomials, and Legendre polynomials).[8] A great many modes are required to accurately recreate a discontinuous function from a set of smooth functions.

Robustness of POD/ROM

POD modes are generated to match the geometry of all the functions that can be created by a linear combination of the set of snapshots. As shown above, replicating discontinuous behavior of functions sampled by the snapshots was no problem for POD.

However, design iteration using POD/ROMs will require POD to produce results where the full order solution wanders outside the original set of candidate snapshots from which the POD/ROM was formed. This is because the set of snapshots is formed using outcomes of the full order CFD representation, which are very expensive (computationally) to generate. The value of the reduced order model will be its ability to generate accurate flow solutions that have not been produced by the full order solver. For low-speed flows, flow structures inherent in POD modes are adequate for a wide range of full order solutions. As a result POD reduced order models are reasonably robust for low-speed incompressible flows.[6] As will be shown, this is not the case for high-speed compressible flows with moving strong discontinuities because POD is a linear method. In other words, a function containing a discontinuity at one location cannot translate that discontinuity to another location under linear addition with another function, unless that second function has a discontinuity at the new location as well. Since POD is a linear technique, for POD to move a shock, both shock locations must reside in the original set of snapshots. It would seem this would require a full order solver solution for every shock location of interest, which might defeat the purpose of the reduced order model.

To illustrate this condition, the POD/ROM from the $100s$ case was used to model a flow field slightly different from the flow field used to form it. Small changes in γ were made to move the steady state shock location incrementally downstream. The steady state solution for density at several values of γ is shown in Figure 7. These results were obtained from the full order model.

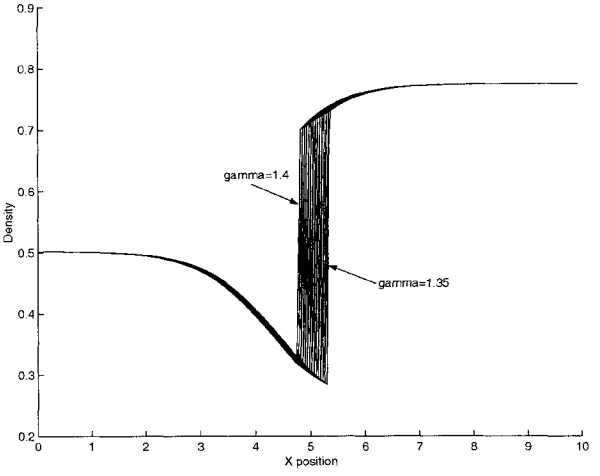

Fig. 7 Shock Motion with Varying γ

Using the same linear initial condition described earlier, the POD/ROM from the $100s$ case was time integrated with the new value of γ. The POD/ROM for the $100s$ case would not converge to a steady state solution for a drop in γ beyond 1.398. For larger drops in γ, the POD/ROM time integrations went unstable during the transient period as the shock attempted to settle at the new downstream shock location. This occurred because the spatial region containing the shock motion captured in the snapshots at $\gamma = 1.4$ did not coincide with the range of shock motion as γ was

reduced. None of the modes in the POD/ROM contained a discontinuity outside the original range of shock motion, so the shock could not be formed at the proper location. As a result, the POD/ROM went unstable.

To further illustrate this lack of robustness, a POD/ROM for the $100s$ case with $\gamma = 1.4$ was created on a refined grid of 250 evenly spaced grid points. Previously, 100 snapshots at $1s$ intervals were adequate to produce a very accurate POD/ROM when the full order solution contained 63 evenly spaced grid points. However, with the grid refined to 250 grid points, no number or combination of modes from a set of 100 snapshots taken at $1s$ intervals would produce a working POD/ROM. In every instance the POD/ROM would go unstable during the time integrations as the shock was moving in the transient period. This instability occurred because the shock motion during the transient period covered a great many more grid points when the grid was refined. Since the modes must contain a discontinuity for every shock location, many more than the 100 snapshots would be required for this POD/ROM to function. Snapshots collection must ensure that a snapshot be taken one grid point at a time for every grid point the shock traverses during the time integration of the full order solver.

These experiments confirmed that current techniques for generating POD/ROMs, as used for low-speed analysis, are inadequate for high speed analysis of flows with moving shocks. POD/ROMs generated this way require a great many snapshots; one for each grid point traversed by a shock wave. POD/ROMs generated in this fashion are not robust to parameter changes in the flow field. Essentially, this POD/ROM would only reproduce solutions which were already obtained from expensive runs of a full order solver. It could never extend the full order results to study new flow field behavior. Such a POD/ROM would have little utility for iterative design analysis.

Domain Decomposition

Domain decomposition is a technique to separate the fluid problem spatially into regions, and isolate the region of the flow experiencing the shock wave. This assumes that the shock is confined to a spatial region of the flow field that can be reasonably identified. For the regions of the flow field not containing a shock, a POD ROM can be generated using the methods developed for low-speed flow problems. No modification to the POD process is required for these regions. The region (or regions) of the flow field containing moving shocks can be approached a number of ways.

One way to deal with this region is to us the full order simulation. Even though the shocked region of the flow has no reduction in the number of DOFs, the use of POD/ROM over the non-shocked portions of the flow field will still provide a significant reduction in the number of DOFs relative to the original problem. Another possibility involves developing a reduced order model for the shocked region of the domain decomposed flow field. POD will be used as a tool to search for a modal representation of this region of the flow field that allows for both order reduction and accurate shock movement. Since the isolated shock domain is a very small portion of the entire solution domain, snapshot collection and POD/ROM development for this region will be more efficient, allowing the reduced order model to be generated without excessive expense.

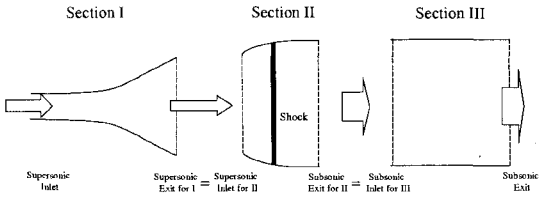

Fig. 8 Domain Decomposition for the Quasi 1-D Nozzle

For the quasi 1-D nozzle problem, the domain was decomposed into three regions as shown in Figure 8. Section I started at the nozzle inlet and ended prior to the shock, thus the flow was supersonic throughout section I. Section II began at the exit of section I and ended after the shock, thus section II had a supersonic inlet and a subsonic exit. Section III consisted of the rest of the nozzle to the exit, and contained all subsonic flow. Section I and III were modeled with POD/ROMs. Both full order and reduced order approaches for section II were studied.

Explicit Analysis and Results

Initially, an explicit time integration of the three sections was used to produce a reduced order solution for the POD/ROM Domain Decomposition (POD/ROM/DD) with a full order section II. Time integration for the POD/ROMs of sections I and III was accomplished using equation (6). To facilitate the simultaneous integration of the three sections, the inlet and exit grid points for section II were coincident with the exit grid point for section I and the inlet grid point for section III. For the $100s$ case with 63 grid points, the explicit POD/ROM/DD was able to accurately reproduce the full order solution with 81 DOFs, down from 189 DOFs for the full order nozzle. For the $30s$ case, there was a smaller range of shock motion so the number of grid points modeled at full order in section II was reduced. For this case the number of evenly spaced grid points was expanded to 250. A very accurate solution was obtained using the following domain decomposition: section I contained 116 grid points, section II contained 9 grid points, and section III contained 125 grid points. The density solution at the time of largest L^2_{err} is shown in Figure 9. This re-

duced order model used 8 modes per fluid variable in sections I and III. Section II contained 9 grid points. The resulting reduced order model had 75 degrees of freedom, down from 750 for the full order problem.

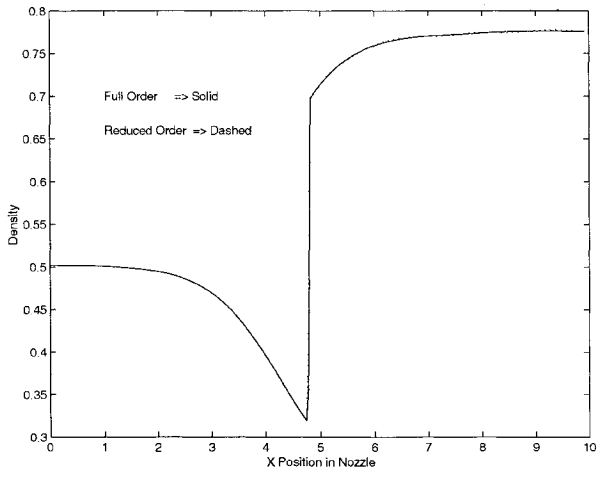

Fig. 9 POD/ROM/DD Density Comparison with 250 Grid Points

Implicit Analysis with Full Order Shock Region

Next an implicit non-Galerkin formulation was developed for the POD/ROM/DD with a full order shock region. Domain decomposition required a reordering of the full order solution vector $\underline{x}(t)$. Instead of ordering the members of $\underline{x}(t)$ by fluid variables distributed spatially across the entire nozzle, $\underline{x}_{DD}(t)$ stacked the fluid variables across each section. Each of the three sections was treated as an independent full order solution $\underline{x}_{S1}$, $\underline{x}_{S2}$, and $\underline{x}_{S3}$, so each had its own reduced order mapping $\underline{x}_{S1} = \Psi_1 \cdot \widehat{\underline{x}}_{S1}$, $\underline{x}_{S2} = \Psi_2 \cdot \widehat{\underline{x}}_{S2}$, and $\underline{x}_{S3} = \Psi_3 \cdot \widehat{\underline{x}}_{S3}$. Since section II was modeled at full order, $\widehat{\underline{x}}_{S2} = \underline{x}_{S2}$ and Ψ_2 was the identity mapping.

The full order Roe's scheme solver was adjusted to consider the each section independently. The output from the Roe solver for each of the three sections was stacked by section, and the resulting vector was denoted as $F(\underline{x}_{DD}(t))$. At full order, Newton's method to obtain the steady state flow field for the domain decomposition ordering is as follows.

$$\frac{dF(\underline{x}^{\nu}_{DD})}{d\underline{x}^{\nu}_{DD}} \cdot (\underline{x}^{\nu+1}_{DD} - \underline{x}^{\nu}_{DD}) = F(\underline{x}^{\nu}_{DD})$$

The domain decomposition reduced order mapping combines each independent section as follows.

$$\underline{x}_{DD} = \begin{bmatrix} \underline{x}_{S1} \\ \underline{x}_{S2} \\ \underline{x}_{S3} \end{bmatrix} = \begin{bmatrix} \Psi_1 & [0] & [0] \\ [0] & I & [0] \\ [0] & [0] & \Psi_3 \end{bmatrix} \cdot \begin{bmatrix} \widehat{\underline{x}}_{S1} \\ \underline{x}_{S2} \\ \widehat{\underline{x}}_{S3} \end{bmatrix}$$

$$\Psi_{DD} = \begin{bmatrix} \Psi_1 & [0] & [0] \\ [0] & I & [0] \\ [0] & [0] & \Psi_3 \end{bmatrix}$$

Substituting the reduced order mapping $\underline{x}_{DD} = \Psi_{DD} \cdot \widehat{\underline{x}}_{DD}$ into the full order Newton's method yields the following reduced order Newton's method.

$$\widehat{\underline{x}}^{\nu+1}_{DD} = \widehat{\underline{x}}^{\nu}_{DD} + \frac{d\widehat{F}(\widehat{\underline{x}}_{DD})}{d\widehat{\underline{x}}_{DD}}^{-1} \cdot \widehat{F}(\widehat{\underline{x}}^{\nu}_{DD})$$

Notice that the reduced order Jacobian can be obtained from the full order Jacobian as follows.

$$\frac{d\widehat{F}(\widehat{\underline{x}}_{DD})}{d\widehat{\underline{x}}_{DD}} = \left(\Psi^T_{DD}\Psi_{DD}\right)^{-1}\Psi^T_{DD}\frac{dF(\underline{x}_{DD})}{d\underline{x}_{DD}}\Psi_{DD}$$

The full order Jacobian $\frac{dF(\underline{x}_{DD})}{d\underline{x}_{DD}}$ was approximated numerically using central differences from evaluations of $F(\underline{x}_{DD})$ about $\underline{x}_{DD} \pm \Delta\underline{x}$. This non-Galerkin implicit method improves numerical efficiency because the reduced order Jacobian requires is more easily inverted . The Jacobian update is still accomplished at full order; however, this update does not need to be accomplished for every Newton iteration. Once the Newton iterations provide a solution sufficiently close, repeated iteration on the same Jacobian will converge quickly within the desired error threshold.

Implicit Analysis with Reduced Order Shock Region

Attempts were made to obtain a solution using a POD/ROM for section II generated from 25 snapshots of steady state flow solutions at values of γ from $1.4 \rightarrow 1.35$ (shown in Figure 7). As γ was increasingly dropped from the 1.4, Newton iterations introduced a non-physical discontinuity at the intersection between sections II and III. Clearly a method to enforce smoothness at this intersection was required to use a POD/ROM for section II with the implicit solver.

This was accomplished using a constrained optimization technique. First, the domains in sections II and III were allowed to overlap by a few grid points. A functional $\ell(\underline{x}_{DD})$ was defined such that $\frac{d\ell(\underline{x}_{DD})}{d\underline{x}_{DD}} = F(\underline{x}_{DD})$. Minimizing $\ell(\underline{x}_{DD})$ was the same as solving $F(\underline{x}_{DD}) = 0$, or finding the steady state solution to the Euler equations for this problem. A constraint was introduced to enforce smoothness at the intersection of sections II and III. A vector T with the same dimensions of $\underline{x}_{DD}$ was defined such that $\underline{x}^T_{DD}T = 0$ when the flow variables for the overlapping sections had the same value. This was achieved by placing a 1 or -1 in each fluid variable location corresponding to the overlap in sections II and III respectively. Zeros were placed everywhere else in T. The dot product of T with $\underline{x}_{DD}$ resulted in cancellation of the fluid variables when the overlapping portion of the solution domain was equivalent. If the overlapping fluid variables were not identical, the dot product produced a small scalar residual.

A LaGrange multiplier λ was used to formulate the following constrained minimization.

$$\underline{y} = \begin{bmatrix} \underline{x}_{DD} \\ \lambda \end{bmatrix}$$
$$G(\underline{y}) = \begin{bmatrix} F(\underline{x}_{DD}) + \lambda T \\ \underline{x}_{DD}^T \cdot T \end{bmatrix}$$

The modified Newton's method at full order was as follows for overlapping domains.

$$\underline{y}^{\nu+1} = \underline{y}^{\nu} + \frac{dG(\underline{y})}{d\underline{y}}^{-1} \cdot G(\underline{y}^{\nu})$$

The modified Jacobian was obtained as follows.

$$\frac{dG(\underline{y})}{d\underline{y}} = \begin{bmatrix} \frac{dF(\underline{x}_{DD})}{d\underline{x}_{DD}} & T \\ T^T & 0 \end{bmatrix}$$

The reduced order mapping was modified as follows to include the reduced order mapping $\underline{x}_{S2} = \Psi_2 \cdot \widehat{\underline{x}}_{S2}$ and the LaGrange multiplier.

$$\underline{y} = \begin{bmatrix} \underline{x}_{S1} \\ \underline{x}_{S2} \\ \underline{x}_{S3} \\ \lambda \end{bmatrix} = \begin{bmatrix} \Psi_1 & [0] & [0] & 0 \\ [0] & \Psi_2 & [0] & 0 \\ [0] & [0] & \Psi_3 & 0 \\ 0 & 0 & 0 & 1 \end{bmatrix} \cdot \begin{bmatrix} \widehat{\underline{x}}_{S1} \\ \widehat{\underline{x}}_{S2} \\ \widehat{\underline{x}}_{S3} \\ \lambda \end{bmatrix} \quad (7)$$

Which was rewritten as follows.

$$\underline{y} = \Psi_\lambda \cdot \widehat{\underline{y}}$$

The modified reduced order Newton's method was then obtained.

$$\widehat{\underline{y}}^{\nu+1} = \widehat{\underline{y}}^{\nu} + \frac{d\widehat{G}(\widehat{\underline{y}})}{d\widehat{\underline{y}}}^{-1} \cdot \widehat{G}(\widehat{\underline{y}}^{\nu})$$

The constrained reduced order Jacobian was obtained from the full order constrained Jacobian as follows.

$$\frac{d\widehat{G}(\widehat{\underline{y}})}{d\widehat{\underline{y}}} = \left(\Psi_\lambda^T \Psi_\lambda\right)^{-1} \Psi_\lambda^T \frac{dG(\underline{y})}{d\underline{y}} \Psi_\lambda$$

Implicit Results

These implicit solution methodologies were successfully used to obtain results for the POD/ROM/DD with shock regions modeled at both full order and with POD/ROM. The 250 grid point full order nozzle problem was decomposed into three sections: section I had 117 grid points, section II had 15 grid points plus 2 coincident grid points for a total of 17, and section III had 118 grid points. Two POD/ROM/DD models were analyzed. The first modeled section II at full order with 17 grid points. Section I used one mode per fluid variable, and section III used one mode for both density and momentum, and two modes for energy. The resulting POD/ROM/DD had 58 DOFs, down from the original 750. The second POD/ROM/DD used a POD/ROM for section II generated from the 25 snapshots of steady state flow solutions at values of gamma from 1.4 $\rightarrow$ 1.35 described earlier. An additional four grid points were added to section II as overlap with section III. The POD/ROMs for sections I and III were identical to that described above for the first case. Upon examination of the eigenvalues associated with the modes for section II, significant energy (order 10^{-3}) was found in the 16^{th} mode. Energy in the 17^{th} mode was order 10^{-7}. Very good results were obtained using 16 modes per fluid variable. The resulting POD/ROM/DD had 55 DOFs, 7 for sections I and III, and 48 for section II.

Steady state solutions from both POD/ROM/DDs were obtained as γ was varied from 1.4 down to 1.37. Note that the POD/ROMs for sections I and III were trained at $\gamma = 1.4$. The ability of both POD/ROM/DDs to track the quasi-steady shock motion is depicted in Figure 10. Notice that both POD/ROM/DDs tracked the shock motion very closely. The POD/ROM/DD with the full order section II misplaced the shock location one grid point down stream as γ was reduced, while the POD/ROM/DD with a POD/ROM for section II tracked shock location nearly exactly to the full order result.

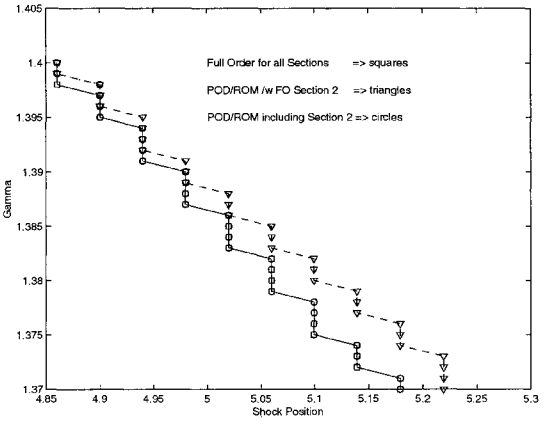

Fig. 10 POD/ROM/DD Shock Location in the Nozzle

Both POD/ROM/DDs accurately recreated the flow solution before and after the shock. Errors in density after the shock for both POD/ROM/DDs are depicted in Figure 11. Notice that errors grew as gamma was steadily decreased, which occurred because the POD/ROMs for sections I and III were trained at $\gamma = 1.4$. Even with the small error growth, the error in density was less than 1% for either the L_2 or the maximum norms.

Errors in density before the shock for both POD/ROM/DDs are depicted in Figure 12. Notice

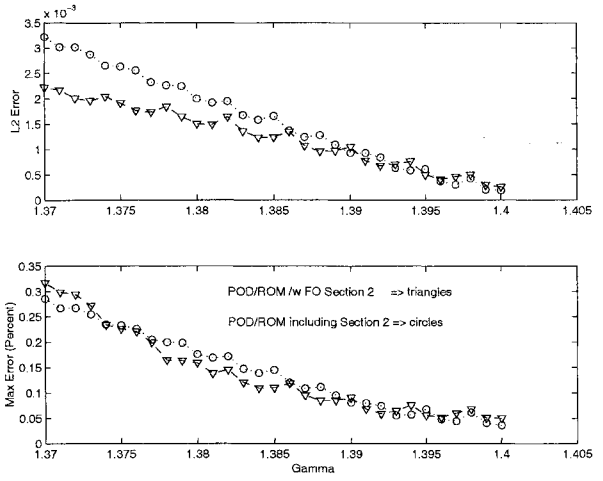

Fig. 11 POD/ROM/DD Density Error After the Shock

that error growth was greater for this portion of the nozzle. Also notice that both POD/ROM/DDs exhibited the same performance. For both models, a small discontinuity formed at the intersection of sections I and II as gamma was steadily decreased. This discontinuity slowly grew as γ was decreased further. The growing discontinuity is reflected in the larger maximum error norm in Figure 12. The constrained implicit formulation did not include overlap between sections I and II, which allowed for the non-physical discontinuity to occur. Future implementations should consider the use of overlap at all domain junctions to eliminate this inaccuracy .

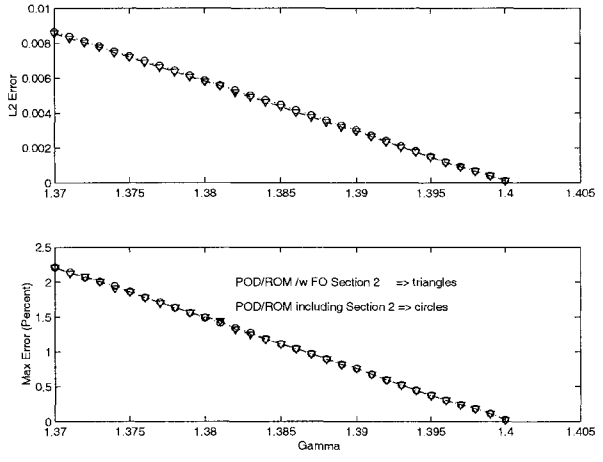

Fig. 12 POD/ROM/DD Density Error Before the Shock

Conclusions

The ability of POD/ROM to replicate the shocked flow solution from which it was formed was demonstrated. It was shown that POD/ROM can accurately recreate a flow solution with strong shocks, given that the appropriate data is present in the matrix of snapshots. If the shock is reasonably stationary, POD/ROM can accurately model the flow field with as few as three modes per fluid variable. It was also shown that the POD/ROM could very accurately reproduce a flow field sequence involving a transition from smooth to shocked flow, including a shock with significant movement. Recreating this case required many more modes for accurate representation.

In high-speed design analysis, shock movement will force the POD/ROM to perform in circumstances beyond the condition under which it was trained. Even small excursions of the shock location beyond the data result in failure of the POD/ROM to arrive at a solution. In these cases the POD/ROM goes unstable attempting to form the shock. The desire to use POD/ROM in design analysis of shocked flows motivates a domain decomposition shock capturing approach. The accuracy and order reduction of the domain decomposition approach was demonstrated for a quasi 1-D nozzle flow. The non-shocked regions of this flow field were modeled using POD/ROM. These POD/ROMs were trained using $\gamma = 1.4$. The shocked region of the flow field was modeled both by POD/ROM and by the full order CFD model adapted for this region. The accuracy of both models was examined for quasi-steady shock motion as γ was varied from $1.4 \rightarrow 1.37$. Both cases produced accurate flow fields and shock motion. Flow field errors were less than 2%, and the shock movement was tracked within one grid point of the true shock location.

Both methods exhibited similar order reduction. The full order solution had 750 DOFs, the POD/ROM/DD with a full order shock region had 58 DOFs, and the POD/ROM/DD with a POD/ROM for the shock region had 55 DOFs. Sixteen modes per fluid variable were required for an accurate POD/ROM of the shocked region, resulting in the insignificant additional order reduction relative to the POD/ROM/DD with a full order shock region. Because of the computational expense of generating snapshots and the large number of modes required, there are no advantages motivating POD/ROM for the shocked region for this 1-D case. However, in 2-D and 3-D cases there might be a significant order reduction gained by constructing a POD/ROM for the regions containing shocks. In such situations, the computational expense of obtaining snapshots could be reduced by using a POD/ROM/DD with full order shock regions to generate snapshots, instead of the full order model.

References

[1]Romanowski, M. C. and Dowell, E. H., "Reduced Order Euler Equations for Unsteady Aerodynamic Flows: Numerical Techniques," *AIAA 96-0528*, 1996.

[2]LeGresley, P. A. and Alonso, J. J., "Airfoil Design Optimization Using Reduced Order Models Based on Proper Orthogonal Decomposition," *Fluids 2000 Conference and Exhibit, Denver, CO (AIAA 200-2545)*, June 2000.

[3]Park, H. M. and Lee, M. W., "An Efficient Method of Solving the Navier-Stokes Equation for Flow Control," *International Journal for Numerical Methods in Engineering*, Vol. v41, 1998, pp. 1133–1151.

[4]Shubin, G., Stephens, A., and Glaz, H., "Steady Shock Tracking and Newton's Method Applied to One-Dimensional Duct Flow," *Journal of Computational Physics*, Vol. 39, 1981, pp. 364–374.

[5]Tannehill, J. C., Anderson, D. A., and Pletcher, R. H., *Computational Fluid Mechanics and Heat Transfer*, Hemishpere Publishing Company, Washington DC, 1997.

[6]Holmes, P., Lumley, J., and Berkooz, G., *Turbulence, Coherent Structures, Dynamical Systems and Symmetry*, Cambridge University Press, 1996.

[7]Beran, P. S., Huttsell, L. J., Buxton, B. J., Noll, C., and Osswald, G., "Computational Aeroelastic Techniques for Viscous Flow," *CEAS/AIAA/ICASE/NASA Langley International Forum on Aeroelasticity and Structural Dynamics, Williamsburg, VA*, June 22-25, 1999.

[8]Canuto, C., Hussaini, M., Quarteroni, A., and Zang, T., *Spectral Methods in Fluid Dynamics*, Springer-Verlag, Berlin, 1988.